



1 **Understanding soil loss in two permanent gully head cuts in the mollisol region of**
2 **Northeast China**

3 Chao Ma¹, Shoupeng Wang¹, Dongshuo Zheng¹, Yan Zhang¹, Jie Tang², Yanru Wen³, Jie Dong⁴

4 1. School of Soil and Water Conservation, Beijing Forestry University, Beijing 100083, PR China.

5 2. Advanced Institute of Natural Sciences, Beijing Normal University at Zhuhai, Zhuhai 519087, China

6 3. Institute of Agricultural Resources and Regional Planning, Chinese Academy of Agricultural Sciences, Beijing
7 100081, China

8 4. Civil and Environmental Engineering Department, Clarkson University, NY, 13699, USA.

9 Corresponding Author: Professor Chao Ma, sanguoxumei@163.com

10 **Abstract:** Gravitational mass wasting on steep slopes plays an important role in permanent gully development. This
11 is typically driven by hydrological processes in the head cut and the hydromechanical response within the soil mass.
12 In this study, erosion intensities were observed in the head cuts of two permanent gullies in the mollisol region of
13 Northeast China during the rainy and snow melting seasons. To understand the physical process, soil water storage
14 and drainage capacity, and suction stress during the 111 d of the rainy season and 97 d of the snow melting season,
15 critical parameters such as soil moisture, temperature, and precipitation were investigated. This analysis also
16 examined the increase in pore water pressure, dissipation properties, and hydromechanical properties of the mollisols.
17 Under the same confining stress, the mollisols in the interrupted head cut of Gully No. II increased more rapidly and
18 dissipated pore water pressure more than at the uninterrupted head cut of Gully No. I. The combination of the soil
19 water characteristic curve and the hydraulic conductivity function indicates that the mollisols of Gully No. II had a
20 higher air entry pressure and saturated hydraulic conductivity during the wetting and drying cycles than Gully No.
21 I. The head cut area of Gully No. II exhibited rapid water infiltration and drainage responses during rain events, with
22 a high soil water storage capacity during torrential rain, rainstorms, and snow melting seasons. The absolute suction
23 stresses within the mollisols of Gully No. II was lower than that in Gully No. I, which could lead to high erosion per
24 unit of steep slope area. Soil loss from gravitational mass wasting on steep slopes is closely related to soil suction
25 stress and we observed a correlation between erosion per unit gully bed area and the soil water storage. These
26 findings have deepened our understanding of the physical process of permanent gully development from the
27 perspective of the hydrological and hydromechanical behavior of gully head cuts.

28 **Keywords:** Gravitational mass wasting; Soil water characteristic curve; Erosion per unit area

29 **1 Introduction**

30 Gravitational mass wasting refers to the downward movement of rock, regolith, and/or soil caused by gravity
31 along the sloping top layers of the earth's surface (Evans, 2004; Allen et al., 2018). There are four types of mass
32 wasting, based on the speed of movement of the material and the level of moisture, namely, falls and avalanches,
33 landslides, flow, and creep (Bierman and Montgomery, 2014). They often occur in various sizes with undetermined
34 failure planes and are affected by hydrological and hydromechanical responses (Stein and LaTray, 2002; Rengers
35 and Tucker, 2014). On the steep slopes of permanent gullies, gravitational mass wasting involves debris-free soil
36 falling owing to bed undercutting driven by intensive channelized flow or persistent high soil moisture (Harmon and
37 Doe, 2001). Soil loss from gravitational mass wasting during the rainy season occurs when a steep slope loses support
38 from debris deposits. Meanwhile, soil loss during the melting season may result from persistent low soil suction
39 stress. In unsaturated soil mechanics, a high occurrence potential or intensive soil loss from gravitational mass
40 wasting corresponds to low soil suction stress (Lu and Godt, 2013). It remains unclear whether soil loss from
41 gravitational mass wasting corresponds to soil suction stress during these two stages.



42 Permanent gullies are initiated in locations where concentrated flows can erode and deliver bed sediments
43 (Kirkby and Bracken, 2009; Sidle et al., 2017) and expand when gravitational mass wasting occurs following instant
44 or constant water infiltration (Poesen et al., 2010; Tebebu et al., 2010). Permanent gully development can be
45 determined by the topographical threshold and volumetric retreat rate of gully head cuts (Svoray et al., 2012; Guan
46 et al., 2021; Zare et al., 2022), the gully length–area–volume relationship (Li et al., 2015 and 2017), and their function
47 in the upstream drainage area and rainy days in different environments (Hayas et al., 2019). Soil loss from permanent
48 gullies is largely influenced by hydrological factors (Gómez-Gutiérrez et al., 2012), such as the flow rate, total water
49 volume, rainfall intensity and amount, and hydromechanical properties of the soil mass. Soil properties are affected
50 by land use, plant roots, texture, and structure. The hydrological process near the head cut, the hydromechanical
51 response of soil mass in reaction to water infiltration, and their relationship with soil loss from gravitational mass
52 wasting remain unknown. Under natural conditions, water infiltrates either following rain events or snow/ice melting
53 events. The infiltration rate strongly depends on both the amount and intensity of precipitation, which leads to soil
54 water storage. However, the amount of stored water varies owing to the amount of rainfall and the melting rate or
55 temperature. During the snow/ice-melting season, the duration of water infiltration persists longer than that of rain
56 events because of prolonged soil saturation and an extended period of low soil suction stress. This may generate
57 more soil loss owing to gravitational mass wasting. However, rain events typically generate intensive channelized
58 flows, which erode steep slopes and trigger gravitational mass wasting. Therefore, it is challenging to compare soil
59 loss in the two seasons. However, this issue could be addressed by considering the associated hydrological processes
60 of head cuts and hydromechanical responses within the soil mass.

61 In the mollisol region of Northeast China (MEC), over 296,000 permanent gullies have developed since 1960
62 (Yang et al., 2017; Dong et al., 2019). Gravitational mass-wasting processes have caused rapid gully widening due
63 to overfarming and a lack of maintenance (Wang et al., 2009). Various studies have focused on the hydrological
64 processes affecting ephemeral gully development and volume disparities caused by rain/snow melting (Tang et al.,
65 2022; Jiao et al., 2023), tillage practices (Xu et al., 2018; Li et al., 2021), and morphology (Zhang et al., 2016).
66 Permanent gullies pose a greater threat to croplands than ephemeral gullies because the soil loss from permanent
67 gully erosion can be as high as 50–65% of the total loss (Zhang et al., 2022). The relatively high area increasing
68 ratio is affected by the combination of permanent gullies with cropland use, a large ridge orientation angle, and a
69 sunny orientation (Li et al., 2016; Liu et al., 2023). Tang et al. (2023) provided evidence of the rainfall threshold for
70 permanent gully development and found that the maximum value of 3 d accumulative rainfall best explained
71 permanent gully bed erosion, and the cumulative value of erosive rainfall best accounted for gravitational mass
72 wasting. However, gravitational mass wasting on the steep slope of a permanent gully can occur either during the
73 rainy season or snow melting season (Zhang et al., 2020; Zhou et al., 2023). Currently, the hydrological processes
74 near the head cut and the hydromechanical response of mollisols to water infiltration in the two seasons have never
75 been documented, and the associated soil loss from gravitational mass wasting is poorly understood. In the MEC,
76 although the duration of the snow/ice melting season is shorter than that of the rainy season (Wang et al., 2021; Fan
77 et al., 2023; Went et al., 2024), the time for snow melting water or rainy water infiltration and the soil water storage
78 and drainage processes are significantly different. Soil water storage may exceed drainage because of continuous
79 meltwater infiltration and limited water drainage paths. Rain infiltration during the summer season temporarily
80 increases and then decreases once the rain event ceases and the water drains. Stored water significantly depends on
81 rainfall events (Farkas et al., 2005; Xu et al., 2018). Therefore, the duration of low soil suction stress, such as high
82 soil moisture, differed substantially between the two seasons. Another effect is channelized water during intensive
83 rainstorms (Wen et al., 2021), which may erode the bed and result in gravitational mass wasting. Therefore, the soil
84 loss from gravitational mass wasting may coincide with the soil suction stress in the snow/ice melting season.
85 Meanwhile, this coincidence may not exist in the rainy season.



86 Soil loss from gravitational mass wasting on the steep slope of a permanent gully is poorly understood in the
87 MEC. To date, relatively few studies have addressed its relationship with the suction stress of the soil mass. This
88 work has focused on soil loss during the rainy and melting seasons in the head cuts of two permanent gullies, where
89 one head cut experiences no human activity, whereas the other does. Soil loss in the head cut area during the rainy
90 and melting seasons was observed. The differences in the physical properties of the mollisols, such as pore water
91 pressure dissipation at a given confining stress, the soil water characteristic curve (SWCC), and the hydraulic
92 conductivity function (HCF), were compared. The soil loss per unit area on the steep slope and gully bed was
93 analyzed for the soil water storage and drainage and the hydromechanical response, respectively. The results of this
94 study deepen our understanding of permanent gully expansion using classical mechanics.

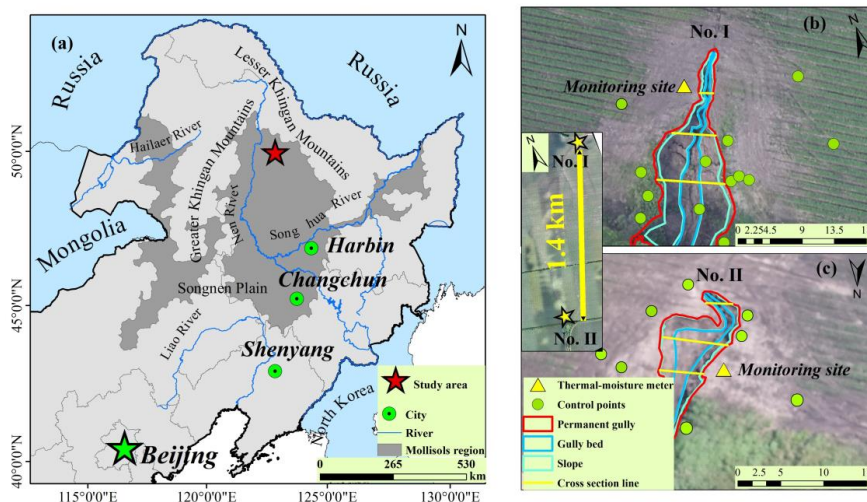
95 2 Study area

96 Northeast China is one of the three main mollisol regions worldwide, with a total area of 1,030,000 km². It
97 contributes 20% of the grain and more than 40% of the corn in China. Most of the mollisol region was gradually
98 converted from native vegetation to cropland beginning in the late 19th Century. Croplands constitute 80% of the
99 total land area, and the main crop types are soybean and corn. The study area is located in the typical heavy gully
100 erosion area of the mollisol region of Northeast China, where native grasslands and forests have been fully converted
101 into croplands since 1968. It is situated in a transitional rolling hilly area extending from the Songnen Plain to the
102 Greater Khingan Mountains in the west, the Lesser Khingan Mountains in the north and near the Nen River (Fig.
103 1a). Owing to the gentle landscape, the farmland in the study area is covered by a thick black organic soil layer, with
104 sandstone, mudstone, and sandy conglomerate underneath.

105 The two permanent gullies examined in this work are 1.4 km apart and are located on the south-facing and
106 north-facing rolling slopes, respectively (Figs. 1b and 1c). The catchment area above Gully No. I is 0.22 km². The
107 relative relief and channel gradient are 25.85 m and 3.3%, respectively. The catchment above the head cut of Gully
108 No. II is 0.35 km², and the relative relief and channel gradient are 26.1 m and 3.2%, respectively. The width of Gully
109 No. I gradually broadened, whereas Gully No. II narrowed and Gully No. I was deeper (Figs. 2a and 2b). The mean
110 depth of the Gully No. I was 3.5 m while that of Gully No. II was 1.23 m. The mean length and width of No. I gully
111 were 25.3 m and 8.72 m, whereas those of Gully No. II were 28.2 and 5.61 m. The gully area for No. I was 199.3
112 m² and the volume was 863.6 m³. For Gully No. I, the area and volume of the gully were 143.3 m² and 123.6 m³.

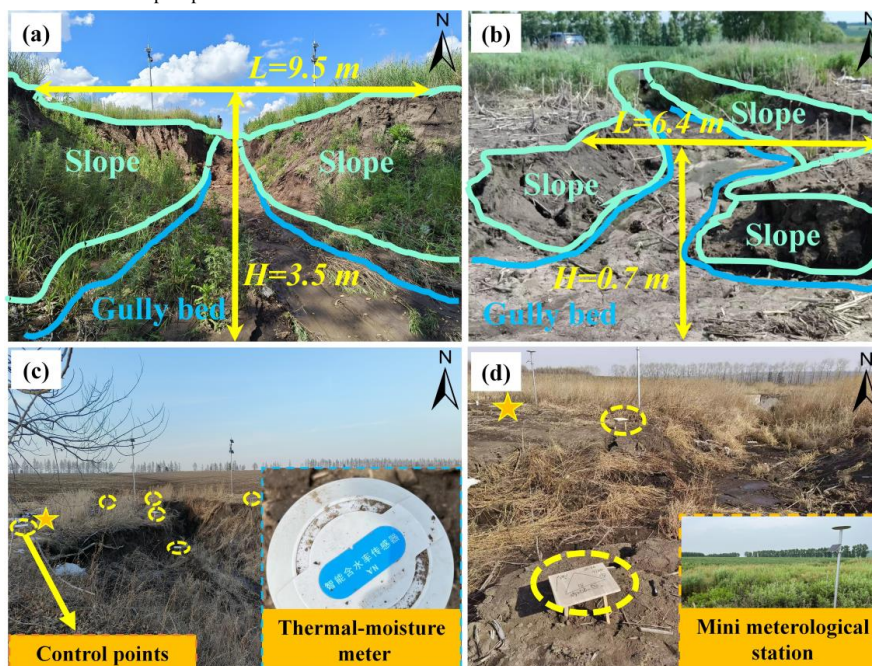
113 The two gullies are still expanding because they are connected to the river network, which drains water into the
114 Nen River. Although grass covers the area near the sidewall and ridge along the gully, mass wasting movement
115 frequently occurs during the melting and rainy seasons. The differences in the gully planform and depth indicate that
116 the mass movement at the sidewall or head cut has distinctive rates and scales. The mass movement at the sidewalls
117 of the two gullies differed in scale, as shown in Figs. 2c and 2d. The height and width of the Gully No. II were lower
118 than those of the Gully No. I (Fig. 3). The head cut area of Gully No. II underwent tillage activities, whereas the
119 head cut area of Gully No. I has not. Therefore, Gully No. II is representative of the initial development stage for a
120 large permanent gully.

121 The study area has a continental monsoon climate with variable annual precipitation ranging from 347 to 775
122 mm, with an average of 546 mm between 1971 and 2018 (Tang et al. 2023). Rainfall mainly occurs between June
123 and August, accounting for 70–90% of the annual precipitation, with an average of 461 mm. Snowfall occurs mainly
124 from November to April, accounting for 10–30% of the annual precipitation. The average temperature in the coldest
125 and warmest months are –22.5 °C and 20.8 °C, respectively, with an annual average temperature of 0 °C.



126
 127
 128
 129
 130
 131

Fig. 1. Location of the two permanent gullies in the mollisol region of Northeast China. (a) The red star marks the observation site in the study area (from ESRI). (b) Monitoring sites and ground controlling points at permanent Gully No. I. (c) Monitoring sites and ground controlling points at permanent Gully No. II. (background of a is from ESRI. The area between the blue lines marks the gully bed, and the area between pink and blue lines marks the steep slope.

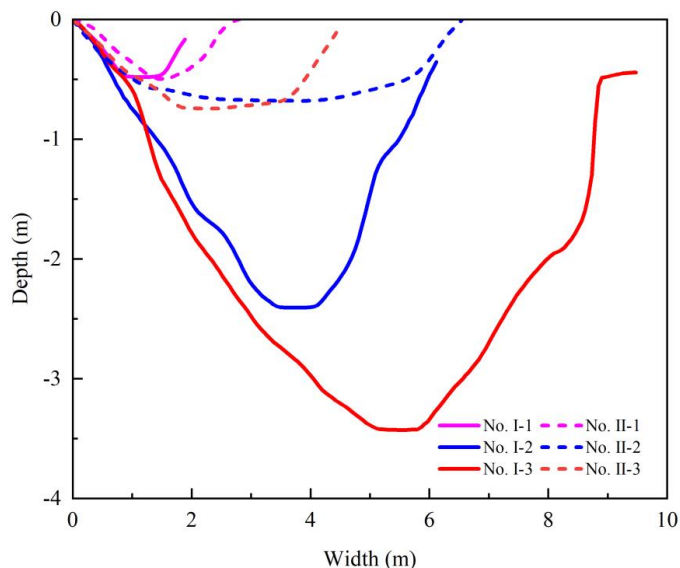


132
 133
 134
 135

Fig. 2. A close view of the steep slope and head cut of the two permanent gullies, with (a) cross-section and upstream view of the permanent Gully No. I, (b) cross-section and downstream view of the permanent Gully No. II, (c) ground control points (blue dot circles) and the soil moisture–temperature monitoring site (yellow star) at



136 permanent Gully No. I, and (d) ground controlling points and the soil moisture–temperature monitoring sites at
137 permanent Gully No. II. The location of the head cut of the two gullies is shown in Fig. 1. The area between
138 the blue lines marks the gully bed. The area between the pink and blue lines marks the slope.



139
140 **Fig. 3.** Difference of the two permanent gullies' cross-section. The location of the cross-section lines is shown in
141 Figs. 1b and 1c.

142 3 Material and methods

143 3.1 Monitoring work

144 Near the gully head cut, frequency–domain reflectometry sensors were installed to monitor the soil moisture
145 and air temperature at depths of 20, 40, 60, and 80 cm (Fig. 2c). These two monitoring sites share the same rainfall
146 records as Gully No. II (Fig. 2d). A trench was dug to obtain soil samples from the two monitoring sites. The soil
147 samples were used for pore water pressure dissipation tests via consolidated undrained triaxial compression tests
148 (CU) using a GDS triaxial apparatus (GDS, UK), and the unsaturated permeability was measured using the transient
149 release and imbibition method (TRIM; Lu and Godt, 2013).

150 To observe the gravitational mass wasting process during the rainy and melting seasons, the study area was
151 scanned using numerous control points (the dots in Figs. 1a and 1b and dashed circles in Figs. 2c and 2d) installed
152 in and around the gully area, and an unmanned aerial vehicle (UAV) was used. These control points were used to
153 improve the accuracy of the UAV-derived map and digital elevation model to obtain highly accurate topography
154 data. Three flights on June 28, 2022, October 17, 2022, and June 20, 2023, were performed with the same flight
155 routine and image overlap. The two frontier flights in 2022 spanned 111 d during the rainy season. The latter two
156 covered the winter of 2022 and spring of 2023. As low soil moisture persists from October each year and snow cover
157 in the winter season does not result in gravitational mass movement, the effective duration of the melting season
158 starts on March 15, 2023. Therefore, the melting season in this study lasted 97 d. We used Pix4D software to process
159 the image synthesis and gully topography production, which can reallocate the point cloud and filter the points of
160 the vegetation layer. As the points of the vegetation layer, mainly the grass blades, are changeable in plant height,
161 whereas the ground point is fixable, the vegetation layer can be filtered out and removed using the filtering tool. The



162 DEM products were spatially registered in ArcGIS 10.2 using a standard layer of orthoimages, ground control points,
 163 and spline functions (Table 1). The erosion depth of the head cut was then obtained from the difference between the
 164 two DEMs. Therefore, the linearity and erosion per unit area could be calculated using the erosion depth and grid
 165 size. The differences between the two digital elevation models generated positive and negative terrain, which showed
 166 soil loss from gravitational mass wasting. The eroded soil volume in a unit of steep slope surface area, termed erosion
 167 per unit area, was applied to address the erosion caused by gravitational mass wasting.

168 **Table 1.** Detailed information of three UAV flights and the digital elevation models

UAV model	Flight date	Season/ duration	Flight height (m)	DEM accuracy (m)	Image overlap (%)
DJI Inspire 2 RTK	2022.06.28	/	200	0.058	80
DJI Phantom 4 RTK	2022.10.17	Rainy/111 d	500	0.108	80
DJI Phantom 4 RTK	2023.06.21	Melting/97 d	150	0.042	80

169 **3.2 Tests of pore water pressure rising and dissipation**

170 The consolidation module of the GDS triaxial apparatus was used to record the pore water pressure within the
 171 soil mass under a given confining stress. The soil samples were initially saturated in a vacuum pump and then
 172 consolidated in the chamber of the GDS apparatus at effective confining pressures of 100, 200, and 300 kPa with a
 173 10-kPa backpressure. The consolidation process was completed when the pore water pressure decreased to the
 174 backpressure values.

175 For the pore water increasing stage:

$$176 P_{\uparrow} = P_0 \times t^{b_{\uparrow}} \quad (1)$$

177 where P_{\uparrow} is the recorded pore water pressure during the increasing stage (kPa), P_0 is the initial pore water pressure
 178 since loading (kPa), t is the time (s), b_{\uparrow} is the rising proxy reflecting the steepness of the power-law curves of pore
 179 water pressure increase.

180 For the pore water dissipation stage:

$$181 P_{\downarrow} = \frac{P_{max}}{1+b_{\downarrow} \times t} \quad (2)$$

182 where P_{\downarrow} is the recorded pore water pressure during the dissipation stage (kPa), P_{max} is the maximal pore water
 183 pressure since loading (kPa) and is the rollover point in the pore water pressure curve, t is the time (s), b_{\downarrow} is the
 184 dissipation proxy reflecting the water drainage ability of soil mass at given confining pressure and reflects the
 185 concavity of the pore water pressure dissipation curve.

186
 187 **3.3 Hydromechanical properties**

188 TRIM was used to test the unsaturated permeability of the soil mass (Lu and Godt, 2013). The SWCC and HCF
 189 were obtained using Hydrus 1-D (Wayllace and Lu, 2012). Using the models proposed by Mualem (1976) and van
 190 Genuchten (1980), the constitutive relations between the suction head (h), water content (θ), and hydraulic
 191 conductivity (K) under drying and wetting states can be represented by the following equation:

$$192 \frac{\theta - \theta_r}{\theta_s - \theta_r} = \left[\frac{1}{1 + (\alpha|h|)^n} \right]^{1 - \frac{1}{n}} \quad (3)$$

193 and

$$194 K = K_s \frac{\left\{ 1 - (\alpha|h|)^{n-1} [1 + (\alpha|h|)^n]^{\frac{1}{n} - 1} \right\}^2}{[1 + (\alpha|h|)^n]^{\frac{1}{2n} - \frac{1}{2n}}} \quad (4)$$



195 where θ_r is the residual moisture content (%), θ_s is the saturated moisture content (%), α and n are empirical
196 fitting parameters, α is the inverse of the air-entry pressure head, n is the pore size distribution parameter, and K_s
197 is the saturated hydraulic conductivity (cm/s).

198 Based on the observed volumetric water content and the SWCC, the suction stress (σ^s , kPa) throughout the
199 observation stage can be expressed as:

$$200 \quad \sigma^s = -\frac{S_e}{\alpha} \left(S_e^{n/(1-n)} - 1 \right)^{1/n} \quad (5)$$

201 3.4 Soil water storage and drainage

202 In this study, the hydrological process of the steep slope is of utmost importance for analyzing gravitational
203 mass wasting because of the varied soil water storage and drainage in the rainy and snow-melting seasons. Soil water
204 is temporally stored during rainstorms, but drains after the rainstorms cease. The drainage process during melting is
205 not addressed herein because melting water constantly contributes to high soil moisture. Therefore, soil water storage
206 (S_s) during rainstorms and the snow-melting season and drainage (S_d) after a rainstorm ceases can be evaluated
207 using the soil depth and the difference between the maximum soil moisture and antecedent soil moisture:

$$208 \quad S_e = \frac{\theta - \theta_r}{\theta_s - \theta_r} \quad (6)$$

$$209 \quad S_s = S_e^w \Delta h_i \quad (7)$$

$$210 \quad S_d = P - S_e^d \Delta h \quad (8)$$

211 where S_e is the degree of saturation, θ is the in-situ observed volumetric moisture content measured (%), Δh_i is
212 the soil layer i (200 mm in this work, $i = 1, 2, 3, 4$), S_e^w and S_e^d are the residual soil moisture in the wetting and
213 drying processes (%), and P is the accumulated rainfall (mm) and equals to 0 mm in the snow-melting season. To
214 show the soil water storage during the rainy and snowmelt seasons, and the water drainage after rainfall, all the
215 information was considered, including rainfall amount, air temperature, soil moisture, and temperature in various
216 soil layers. The recorded rain events were categorized into four groups, that is, light rain, moderate rain, torrential
217 rain, and rainstorms, with rain amounts of < 10, 10–25, 25–25, and 50–100 mm, respectively.

218 4. Results

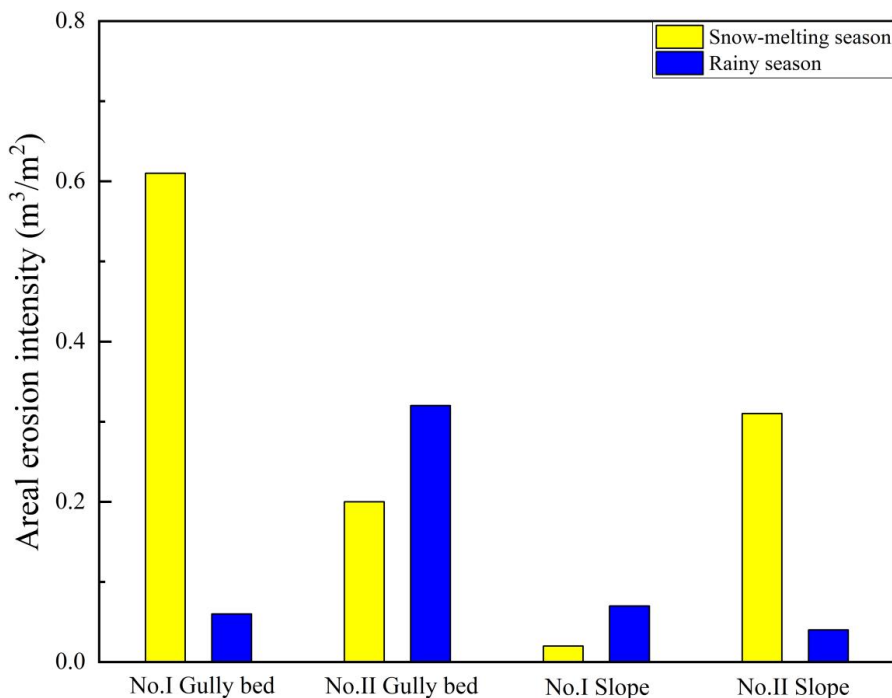
219 4.1 Erosion per unit area of gully bed and slope

220 The erosion per unit area in both bed and slope areas during the snowmelt season for Gully No. I was greater
221 than that in Gully No. II (Fig. 4). This could have been driven by the low meltwater storage and high meltwater
222 runoff at the head cut of Gully No. I. During the rainy season, the erosion per unit area for bed of Gully No. II was
223 greater than that of Gully No. I. This may have resulted from rapid soil water storage and drainage producing
224 intensive runoff at the head cut of Gully No. II. The erosion of steep slopes is mainly due to gravitational mass
225 wasting. For Gully No. II, erosion per unit area during the snowmelt season was significantly greater than that during
226 the rainy season. During the snow melting season, the erosion per unit area for the slope in Gully No. II was greater
227 than that in Gully No. I. Although erosion per unit area during the rainy season for Gully No. I was higher than that
228 of Gully No. II, the difference was negligible compared to that in the snow-melting season. The slopes of the
229 permanent gully were steep, and the stability of the slope primarily depended on the soil suction stress as a function
230 of the hydromechanical properties and the soil moisture.

231 As the channel bed erosion was closely correlated with the hydrological process and the slope erosion
232 corresponded to the soil suction stress, further examination of the associated soil water storage and drainage and the
233 hydromechanical properties of the soil mass in the two permanent gullies was conducted. One of the differences in
234 the hydrological processes in the head cut indicates that soil water storage and drainage occur during the rainy season.
235 Water drainage was absent during the snowmelt season. These results are due to the continuous melting of water



236 from snow and ice in macropores and fissures. Once the melting process was completed, the soil water storage
 237 process ceased with the onset of the water drainage process during the transition time between the snow melting and
 238 rainy seasons.



239
 240
 241

Fig. 4. Differences in the erosion per unit area for the gully bed and slope

Table 2. The physical properties and pore water pressure changes in the soil mass

Parameters	Definition	Confining pressure (kPa)	Permanent gully	
			No. I	No. II
v_{\uparrow} (kPa/min)	Pore water rising ratio	100	11.83	23.04
		200	4.86	90.52
		300	5.55	10.92
b_{\uparrow}	Pore water rising proxy as Eq. (1)	100	0.23	0.25
		200	0.24	0.46
		300	0.30	0.41
v_{\downarrow} (kPa/h)	Pore water dissipation ratio	100	3.68	22.77
		200	3.32	194.47
		300	3.66	23.94
b_{\downarrow} ($\times 10^{-5}$)	Pore water dissipation proxy as Eq. (2)	100	9.97	79.70
		200	7.80	79.40
		300	6.82	18.10
c (kPa)	Effective cohesion		11.3	7.2
φ ($^{\circ}$)	Effective friction angle		16.3	21.3
γ (kN m^{-3})	Unit weight		14.1	12.5

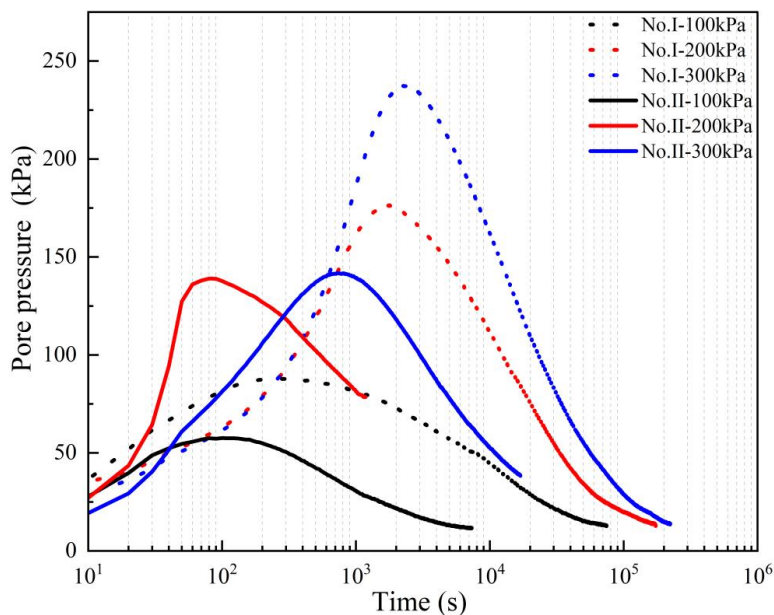
242



243 4.2 Physical properties of mollisols

244 4.2.1 Pore water pressure rising and dissipation

245 Under the same confining pressure, pronounced differences were observed in the rising and dissipation ratios
246 of the pore water pressure within the mollisols of the two gullies. The pore water pressure results during the
247 consolidation process at effective confining pressures of 100, 200, and 300 kPa were compared (Fig. 5). The physical
248 properties, and the rising and dissipation ratios and proxies are listed in Table 2. The peak value of the pore water
249 pressure within the mollisols of Gully No. I was higher than that in Gully No. II. The peak value of the pore water
250 pressure within the mollisols of Gully No. II increased to 57.6, 139.0, and 141.7 kPa under the confining stresses of
251 100, 200, and 300 kPa, respectively. In contrast, the peak value of the pore water pressure within the mollisols of
252 Gully No. I increased to 87.9, 176.1, and 237.3 kPa, respectively.



253

254 **Fig. 5.** Variation in pore water pressure under effective confining pressure of 100, 200, and 200 kPa by GDS
255 triaxial shear tests (GDS Instruments, UK). The proxy for the pore water pressure rising and dissipation are
256 calculated using Eqs. (1) and (2). The rising and dissipation ratio is calculated using the pore water pressure
257 difference during a given time interval. The values of proxy and ratio are shown in Table 2.

258 The high peak pore water pressure illustrates that the mollisols of Gully No. II had strong hydraulic conductivity
259 as the ratio increased, and the proxy and dissipation ratio and proxy represented the pore connectivity. During the
260 rising stage, the rising ratio of the mollisols in Gully No. II was 2 to 18.6 times greater, and its rising proxy was 1.08
261 to 1.92 times larger than that of Gully No. I. Within the dissipation stage, the ratios were 6.20 to 58.6 greater, and
262 its proxies were 2.65 to 8.0 times larger than those for mollisols of Gully No. I. The largest difference between these
263 two gullies was observed under a confining stress of 200 kPa. Therefore, the increase in the pore water pressure and
264 dissipation properties suggests that the head cut of Gully No. II may have exhibited active hydrological processes.

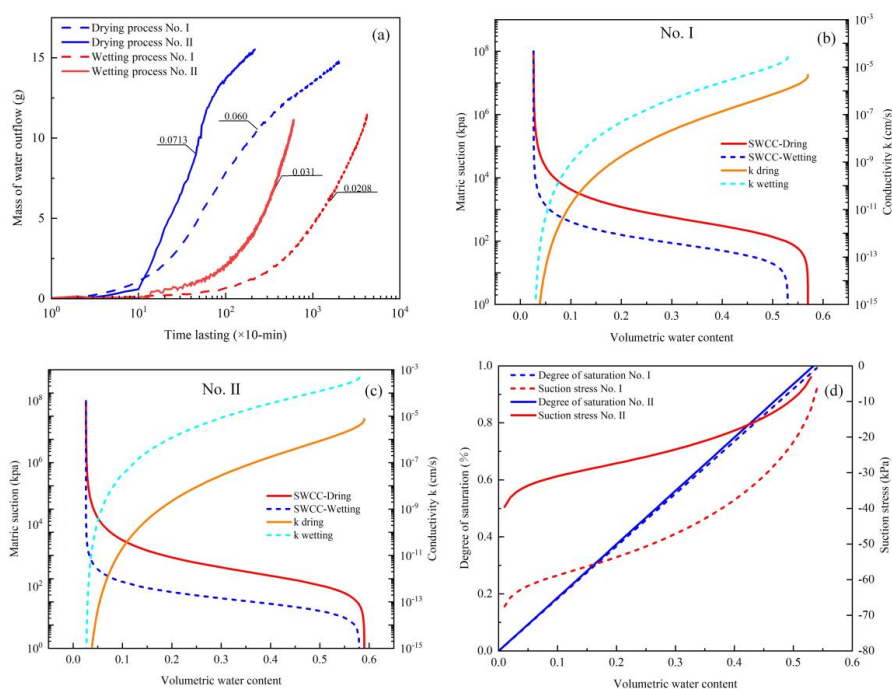
265

266

267 4.2.2 Hydromechanical properties of mollisols



268 Fig. 6 shows the results of the TRIM tests, SWCC, HCF, and estimated suction stress with varying degrees of
 269 saturation. The water outflow mass was measured at 10-min intervals during the drying and wetting processes. The
 270 water outflow masses measured for the mollisols in Gully No. II were generally higher than those of the mollisols
 271 in Gully No. I. For the drying tests using mollisols from Gully No. II and No. I, the water outflow masses were
 272 0.0713 and 0.060 g per 10 min, respectively. For the wetting tests, the water outflow masses were 0.031 and 0.0208
 273 g per 10 min, respectively (Fig. 6a). Overall, the permeability of mollisol Gully No. II was higher than that of mollisol
 274 Gully No. I. The same results were obtained for the pore water pressure increase, dissipation ratio, and proxy, as
 275 shown in Table 2.



276
 277 **Fig. 6.** Differences in the hydromechanical properties of the two soil masses. (a) Water flow mass in the drying and
 278 wetting process. (b) SWCC for soil mass of permanent Gully No. I. (c) SWCC for soil mass of permanent Gully
 279 No. II. (d) Suction stress–volumetric water content curves for the two soil masses. The mass of water outflow
 280 was recorded at 10 min for each test.

281
 282 Using the parameters listed in Table 3, the SWCC and HCF curves of the mollisols were plotted (Figs. 6b and
 283 6c). Air entry pressure and residual water content are two important parameters that describe the hydrological and
 284 mechanical characteristics of mollisols. The air entry pressure represents the critical value at which air enters the
 285 saturated soil and begins to drain. In comparison, the values of α^d and α^w together prove that the required air entry
 286 pressure for mollisols in Gully No. I was greater than that in Gully No. II, and the differences were 79.4 kPa and
 287 28.0 kPa under drying and wetting conditions, respectively (Table 3). Therefore, water infiltration into Gully No. II
 288 during either the rainy or snow melting seasons was more active than in Gully No. I. The residual moisture did not
 289 vary markedly owing to the similarity in the soil types.

290 The saturated hydraulic conductivities of the mollisols in Gully No. I were lower than those in Gully No. II in
 291 both the drying and wetting processes. In Table 2 and Fig. 5, the pore water pressure rising ratio and proxy and the



292 dissipation ratio and proxy further indicate that the permeability of the mollisols in Gully No. II was higher than that
 293 in the mollisols of Gully No. I. Therefore, the pore water pressure changed with varying confining stress, air entry
 294 pressure, and saturated hydraulic conductivities under drying and wetting conditions, suggesting that it is more
 295 challenging for the mollisols in Gully No. I to absorb and drain more water compared to mollisols in Gully No. II.

296 Figs. 6b and 6c present the matric suction and hydraulic conductivity at various soil moisture levels. However,
 297 it was not possible to compare the level of suction stress with various hydrological and mechanical parameters, as
 298 listed in Table 3. Hence, the suction stress at various soil moisture levels was determined (Fig. 6d). The absolute
 299 suction stress at the specified soil moisture for mollisols in Gully No. I was higher than that of mollisols in Gully
 300 No. II, suggesting a higher possibility of gravitational mass wasting for the mollisols in Gully No. II.

301
 302 **Table 3.** Parameters describing the SWCC and the HCF from Hydrus 1D.

Parameters	Definition	Permanent gully	
		No. I	No. II
θ_r	Residual moisture	0.0262	0.0259
θ_s^d	Saturated moisture	0.57	0.59
θ_s^w		0.53	0.58
α^d (kPa ⁻¹)	The inverse of the air entry pressure head	0.0042	0.0063
α^w (kPa ⁻¹)		0.0183	0.0375
n^d	The pore size distribution parameter	1.69	1.68
n^w		1.95	1.91
K_s^d (cm s ⁻¹)	Saturated hydraulic conductivity	4.73×10^{-6}	7.82×10^{-6}
K_s^w (cm s ⁻¹)		2.64×10^{-5}	4.26×10^{-4}

303 Notes: the superscript *d* and *w* indicate drying and wetting states.

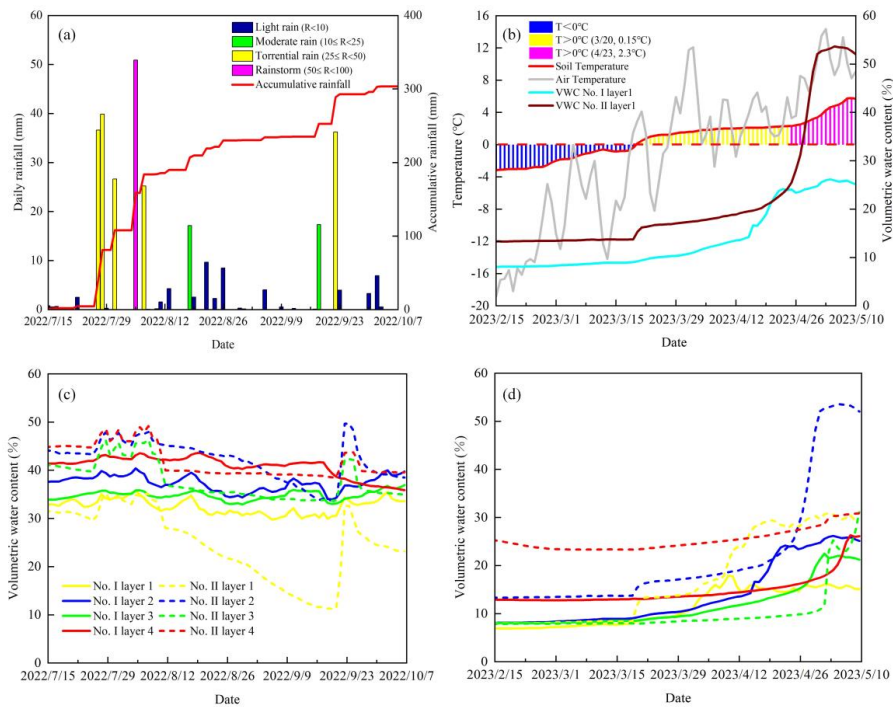
304 4.3 Hydrological response

305 4.3.1 Monitoring results

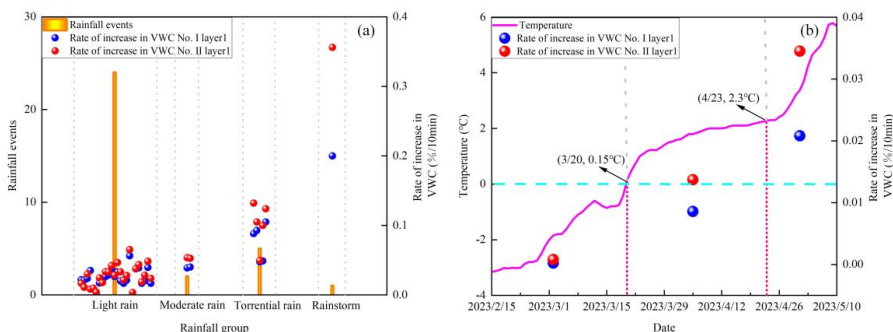
306 In total, 24 light rain events, two moderate rain events, five torrential rain events, and one rainstorm event were
 307 recorded (Fig. 7a). During the snow melting season, the air temperature started to increase above 0 °C on March 20
 308 with an increasing gradient of 0.15 °C per day, which reached 2.3 °C per day after April 23 (Fig. 7b). For soil
 309 moisture changes, the volumetric water content at a depth of 20 cm for Gully No. II greatly increased from April 23,
 310 whereas it only slightly increased for Gully No. I. This suggests that the head cut of the Gully No. II may have
 311 experienced higher soil moisture levels. Soil moisture throughout the rainy and snowmelt seasons had dissimilarities
 312 between sites. During the rainy season, the volumetric water content at a depth of 20 cm persistently remained at a
 313 lower level of soil moisture than at the other three soil depths, as shown in Fig. 7c. However, during the snow melting
 314 season, the volumetric water content of the 40 cm soil layer was the highest (Fig. 7d). Overall, the soil moisture
 315 content of Gully No. II, in both the rainy and snowmelt seasons, exhibited greater fluctuations than Gully No. I.
 316 Water infiltration from rain events or snowmelt into the head cut of Gully No. II was more active than that of Gully
 317 No. I. The observed difference proves that the stored and drained water from the head cut of Gully No. II was
 318 significantly greater than that in Gully No. I.
 319



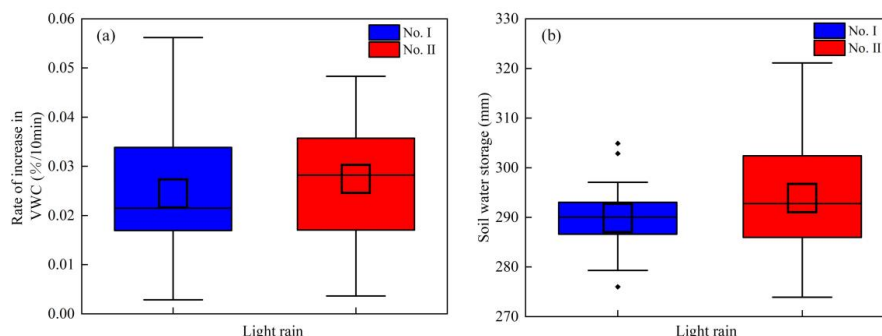
320 To further analyze the differences in water infiltration during the rainy and snowmelt seasons, the rate of soil
 321 moisture increase at a depth of 20 cm was compared in detail (Fig. 8). Among the four types of rain events, the mean
 322 rate of increase for Gully No. II were 0.027, 0.053, 0.102, and 0.356, respectively, which were 1.12, 1.35, 1.34, and
 323 1.78 larger than those for Gully No. I (Figs. 8a and 9a). During the snow melting season, the soil moisture increase
 324 ratios in the initial, medium, and final stages for Gully No. II were 3.48, 1.60, and 1.66 times, respectively, than
 325 those in Gully No. I (Fig. 8b). Therefore, the water infiltration ratios for the head cut areas of Gully No. II during
 326 the rainy and snowmelt seasons.



327
 328 **Fig. 7.** Field-monitored rainfall conditions, air and ground temperature, and volumetric water content. (a) Rain
 329 events during the rainy season. (b) Soil, air temperature, and volumetric water content during the snow melting
 330 season. (c) and (d) Monitored volumetric water content during the rainy season and snow melting season.



331
 332 **Fig. 8.** Volumetric water content increasing ratio in snow melting ratio and the rainy season. (a) Rate of increasing
 333 of VWC at varied rain events. (b) Rate of increase in VWC at three stages of temperature increase.



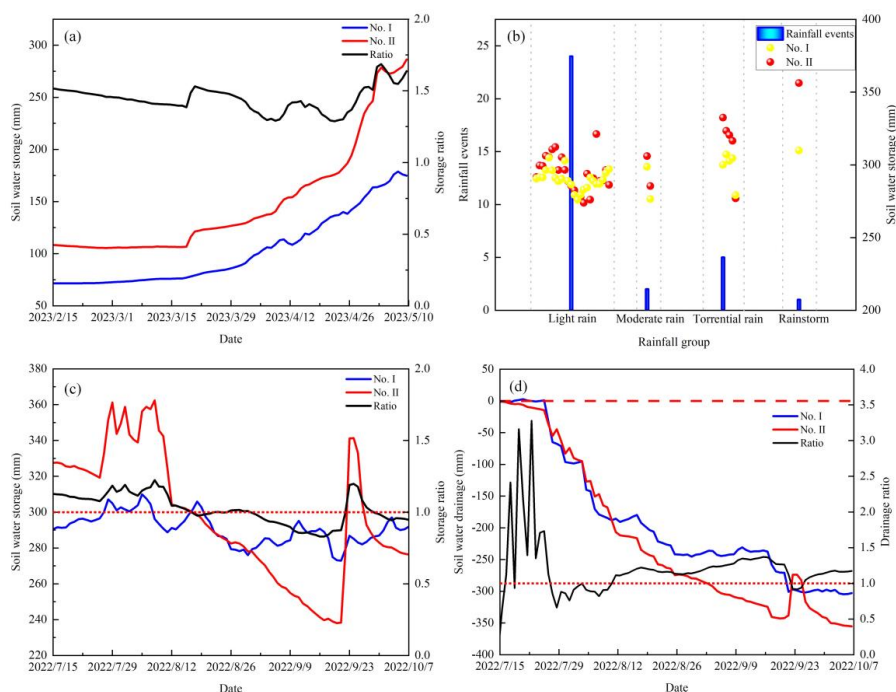
334
335 **Fig. 9.** Hydrologic behavior for gully head cut during light rain events. (a) Lower rate of increase in VWC for Gully
336 No. I. (b) Higher soil water storage for Gully No. II. The three crossing lines of the boxes show the 75th quantile
337 (Q_3), median (Q_2), and 25th quantile (Q_1) from top to bottom. The length of the box is referred to as the
338 interquartile range ($IQR = Q_3 - Q_1$). The crossed square inside the box is the average value. The upper limit
339 and lower limit of whiskers are $Q_3+1.5IQR$ and $Q_1-1.5IQR$, respectively. The solid squares are the outliers.

340 4.3.2 Soil water storage and drainage

341 Fig. 10 shows the stored and drained water in the soil column at the head cuts of the two gullies. During the
342 snowmelt season, the water stored in Gully No. II was higher than that in Gully No. I. The stored water ratio was
343 calculated by dividing the amount of water stored in Gully No. II based on the amount stored in Gully No. I was
344 typically larger than 1.0 throughout the snowmelt season (Fig. 10a). This ratio increased abruptly from April 26.
345 Therefore, the amount of water stored in the head cuts of Gully No. II was higher.

346 Regarding the four types of rain events, the mean stored water for the head cuts of Gully No. II during the 24
347 light rain events was greater than that in Gully No. I (Figs. 9b and 10b). The differences in water stored in the head
348 cuts of the two gullies were 4.0, 8.1, 15.2, and 46.3 mm, respectively. Therefore, the stored water, either in the snow
349 melting season or rainy season, was higher in the head cuts of Gully No. II. However, the water stored in the head
350 cuts of Gully No. II was not always higher than that in Gully No. I, as shown in Fig. 10c. From August 26 to
351 September 3, 2022, the water stored at the head cut of Gully No. II was lower than that in Gully No. I. This could
352 be attributed to high temperatures and light rain events. However, the water stored in the head cuts of Gully No. II
353 exceeded that of Gully No. I during a torrential rainfall event on September 22. The soil water storage capacity of
354 Gully No. II has stronger fluctuations. Rapid water infiltration generally occurs with rapid water drainage. Fig. 10d
355 shows the water drainage and drainage ratios of the two gullies during the rainy season. The water drained from
356 Gully No. II was higher than that in Gully No. I. Therefore, the head cut area of the Gully No. II had better soil water
357 storage capability in snowmelt and rainy seasons and more rapid water drainage in the rainy season than Gully No.
358 I.

359 In summary, rapid soil water storage and drainage for the head cuts of Gully No. II during torrential rain or
360 rainstorms coincided with both the observed pore water pressure rise and dissipation and the hydromechanical
361 properties of mollisols. The high permeability of mollisols at the head cut of Gully No. II was attributed to more
362 rapid soil water storage, drainage processes, and stored water. This could have a considerable influence on the
363 erosion intensity of the steep slope and gully bed of the permanent gully.



364

365

366

367

368

369

370

Fig. 10. Hydrological response during the rainy and snow melting season. **(a)** Soil water storage and the storage ratio during the snow melting season. **(b)** Soil water storage at varied rain events. **(c)** Soil water storage and the storage ratio for the two permanent gullies. **(d)** Soil water drainage and the drainage ratio during the rainy season. During the rainy season, soil water storage and drainage synchronously change with the onset and end of rainfall.

371

4.4 Hydromechanical response and soil loss

372

As the mollisols in the head cut area of the two permanent gullies differed in hydromechanical properties, the monitored soil moisture varied greatly in the field. The suction stress was estimated according to the field-monitored soil moisture at each site and the relationship between the soil moisture and matric suction (Figs. 6d, 7c, and 7d). During the rainy season, the absolute value of the suction stress of the mollisols in Gully No. II was lower than that of Gully No. I (Fig. 11a). The smaller absolute values of the suction stress for the mollisols of Gully No. II during the snowmelt season (Figure 11b). Moreover, the smaller suction stress in the snowmelt season may have resulted in strong erosion on the slope of Gully No. II, as shown in Fig. 4.

378

379

380

381

382

383

384

385

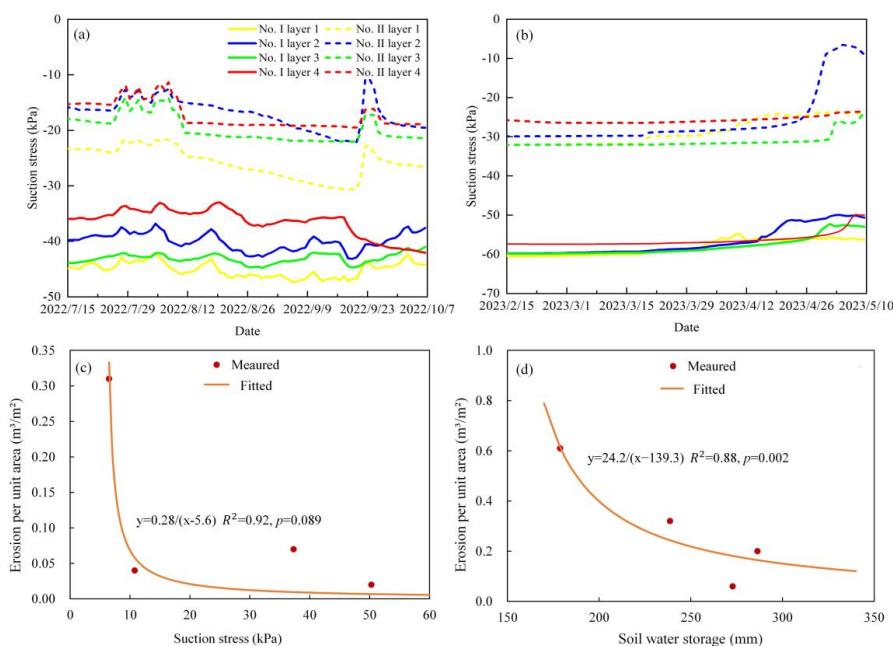
386

387

As the hydrological process of the head cut area is closely related to channel bed erosion, the hydromechanical response influences slope stability. It is important to analyze the possible relationship between the erosion per unit area on the channel bed, soil water storage, and erosion of a steep slope with suction stress. In general, a high absolute value of the suction stress is associated with strong cohesive forces between the soil particles, which is a sign of stability. In contrast, a low absolute value of suction stress suggests a higher potential for slope failure. Therefore, the relationship between the absolute value of the suction stress and erosion per unit area could be negative. Fig. 11c shows the reciprocal relationship between the suction stress and erosion per unit area of the slope. The empirical relationship indicates that gravitational mass wasting occurred on the slope, and the permanent gully expanded when the suction stress remained relatively low for a prolonged period, particularly at approximately 5.6 kPa for the study area.



388 Erosion of the channel bed is closely related to runoff discharge during erosive rain events. During erosive rain
 389 events, the amount of stored soil water decreases runoff amount and intensity. The less rainwater stored during
 390 erosive rain events, the higher the runoff amount, or the more intensive the channeled flow. Therefore, the
 391 relationship between the soil water storage and erosion per unit area of the channel bed could be negative. Fig. 11d
 392 shows the reciprocal relationship between erosion per unit area of the channel bed and soil water storage. It indicates
 393 that excessive rainwater in erosive rain events could create intensified channeled flow to erode the channel bed if
 394 the stored water in the mollisols reached a threshold, such as 139.3 mm in this study area.



395
 396 **Fig. 11.** Relationship between hydrology and the hydromechanical state with the erosion per unit area over
 397 approximately 3 months. **(a)** Suction stress during the rainy season. **(b)** Suction stress during the snow melting
 398 season. **(c)** erosion per unit area on the slope decreases with suction stress. **(d)** erosion per unit area on the
 399 channel bed decreases with soil water storage amount. The time for the monitored rainy and melting seasons
 400 were 111 d and 97 d.

401 5 Discussion

402 The physical processes of permanent gully development can be categorized into gravitational mass wasting on
 403 steep slopes and sediment delivery on channel beds (Montgomery and Dietrich, 1992; van Beek et al., 2008; Luffman
 404 et al., 2015). Traditionally, most studies on gully erosion have focused on soil loss owing to water erosion and piping.
 405 Soil loss estimation is typically determined by several primary factors, such as the upslope contributing area,
 406 topographic conditions, erosive rainfall factors, and land use conditions (Li et al., 2015; Xu et al., 2017; Wang et al.,
 407 2021; Tang et al., 2022). The physical mechanics of bed erosion and slope erosion are different, making it
 408 challenging to accurately predict soil loss on steep slopes. The gravitational mass wasting process on a slope differs
 409 from that of rainfall-induced shallow landslides, especially for those without failure planes (Poesen et al., 1998; Guo
 410 et al., 2020). However, they share similarities, such as a decrease in soil strength due to water infiltration (Guo et al.,
 411 2019). Thus, a thorough mechanical analysis is necessary to understand the physical processes of gravitational mass



412 wasting on the slope and sediment delivery on the channel bed.

413 This study thoroughly investigated the effects of hydrological factors and hydromechanical properties on soil
414 loss on both slopes and channel beds. Mass failure on the hillslopes was governed by suction stress. Meanwhile,
415 erosion on the channel beds was influenced by the soil water storage or runoff amount. Therefore, hydrological
416 factors related to soil water storage and drainage were analyzed (Fig. 10), along with volumetric changes at various
417 rain events and snow melting stages (Fig. 8). In this study, we also investigated the hydromechanical properties and
418 pore water pressure at a given confining stress (Table 2 and Fig. 5), the relationship between the saturation degree
419 and suction stress (Fig. 6), and estimated the suction stress variation during the rainy and snow melting seasons (Figs.
420 11a and 11b). Field observations revealed two permanent gullies with distinct erosion on the slope and gully beds.
421 Gully No. II shows signs of head cut disruption, in contrast to Gully No. I, resulting in disparities in erosion per unit
422 area for both seasons and sites. The hydromechanical properties of the mollisols are distinct between the two gullies,
423 directly affecting water movement. This is evident from the increase in pore water pressure, dissipation ratio, and
424 proxy. In the head cut of Gully No. II, the mollisols were significantly disturbed, and the soil mass had higher
425 permeability and lower suction stress at a given saturation degree. This finding indicates more active water
426 infiltration compared to Gully No. I was triggered by changes in the soil's capacity to store and release water and
427 the higher volumetric water content increasing ratio. Therefore, the head cut area of Gully No. II underwent more
428 aggressive hydrological processes. Additionally, the observed rainfall amount of 139.3 mm in this study was smaller
429 than 177 mm proposed by Tang et al. (2023). This could be explained by the different capacities for plant interception
430 and depression detention during the rainy season.

431 The soil water storage and drainage capacity at the head cut considerably influenced soil loss. Although this
432 study focused primarily on soil water storage and its impact, runoff was not addressed. The soil water storage and
433 runoff depth were approximately equal to the rainfall depth from the perspective of water balance. Consequently,
434 the erosion per unit area of the channel bed was inversely proportional to the soil water storage, as shown in Fig.
435 11d. Some researchers have identified factors leading to the erosion of mass failures on steep slopes, such as long-
436 duration storms (Xu et al., 2020), initial soil moisture in the pre-winter season (Wen et al., 2024), presence of tensile
437 crack morphology (Zhou et al., 2023) and heaving and thawing (Thomas et al., 2009). The head cut of Gully No. II
438 has a high level of disturbance, which may result in higher permeability, quicker water pressure response, and higher
439 soil moisture during either the rainy or snowmelt seasons. Meanwhile, the soil suction stress was lower, and slope
440 erosion was more intense than that of Gully No. I. The distance between the two gullies was only 1.4 km and the
441 climatic conditions were similar. Therefore, soil properties may be the dominant intrinsic factors governing soil loss
442 on gully slopes.

443 Long-term saturation during the snowmelt season provides sufficient water infiltration and low suction stress.
444 Therefore, the highest erosion per unit area occurred in the snowmelt season, but not in the rainy season (Fig. 11c).
445 This was because of the longer duration of snowmelt compared to rain events (Figs. 7a and 7b). Dong et al. (2011)
446 revealed that a critical mass water content for gravitational mass wasting ranged from 31.0% to 33.8%,
447 corresponding to a volumetric water content of 39.0% to 48.0% for the soil mass and a suction stress of 11.0 kPa.
448 This showed that the direct-shear apparatus limited the ability to differentiate between the effective cohesion and
449 suction stress contributions to total cohesion. As shown in Fig. 10b and supported by Xu et al. (2020), the high soil
450 water storage during the snow melting season in Gully No. II (Fig. 9a) and long-term water infiltration can result in
451 lower suction stress and higher erosion per unit area. This suggests a potentially reciprocal relationship between the
452 absolute suction stress and erosion per unit area. As shown in Fig. 10, the accuracy of the two empirical equations
453 can be improved by incorporating data from additional monitoring sites or extending the study period to cover
454 multiple rainy-snow seasons.



455 **6 Conclusions**

456 Permanent gully development is a hydrogeomorphic phenomenon, and its physical mechanics can be attributed
457 to the hydrological and hydromechanical responses of the head cut. In the mollisol region of Northeast China,
458 numerous studies on gully development have focused on soil loss in response to rainfall or snow depth. However, to
459 date, relatively few studies have addressed the physical mechanics of gravitational mass wasting. This study has
460 provided a complete analysis of soil loss on steep slopes and channel beds in two permanent gullies according to
461 hydrological processes, such as infiltration, soil water storage, and drainage, and hydromechanical responses, such
462 as changes in suction stress levels. The following conclusions were drawn:

463 (1) Mollisols in the head cut areas of Gully No. II exhibited a higher permeability than Gully No. I. This can be
464 attributed to the elevated ratio and proxy for pore water pressure rise and dissipation. The TRIM test results
465 confirmed that the saturated mollisols in the Gully No. II drain faster than Gully No. I, owing to their higher air entry
466 pressure and saturated hydraulic conductivity during the wetting and drying cycles.

467 (2) The head cut area of Gully No. II exhibited more intense hydrological processes than Gully No. I. This
468 could be explained by the higher ratio of soil moisture increase observed during the four rain event types and three
469 snow melting stages. Soil water storage in Gully No. II experienced greater fluctuations during torrential rains and
470 rainstorms. Overall, the absolute suction in Gully No. II remained lower than that in Gully No. I, potentially
471 triggering greater erosion on the steep slopes.

472 (3) The relationships between erosion per unit area on the steep slope and channel bed were analyzed for the
473 suction stress and soil water storage. Our findings indicate that low suction stress and high soil water storage can
474 lead to increased gravitational mass wasting while reducing erosion on the channel bed. The two empirical
475 relationships and their efficiency can be improved by incorporating data from ongoing monitoring efforts to enhance
476 the prediction of future soil loss.

477 **Acknowledgements**

478 All authors declare that no conflict of interest exists. This work was study was supported by the National Key
479 Research and Development Program (Grant No. 2021YFD1500700). The authors extend their gratitude to the
480 colleges at the Jiusan Soil and Water Conservation Experimental Station, Beijing Normal University, for their help
481 during field investigations.

482 **Code/Data availability**

483 Any readers can contact Prof. Chao Ma as the corresponding author is willing to share the raw/processed data.

484 **Author contributions**

485 Prof. Ma launched this work based on his skills in gravitational mass-wasting and unsaturated soil mechanics, and
486 proposed the idea-ology of hydrology and hydro-mechanical condition in analyzing the gravitational mass-wasting.
487 Under the guidance of Prof. Ma, Mr. Dongshuo Zheng and Shoupeng Wang finished indoor tests of soil strength and
488 hydraulic-mechanical properties. Prof. Zhang helped determine the field observation sites. Dr. Dong gave insightful
489 comments. Dr. Jie Tang and Yanru Wen provided the research progress about the gravitational mass-wasting on gully
490 expansion in the study area.

491 **Competing interests**

492 All authors have declared that there were no conflicts of interests and competing interests.



493 **References**

- 494 [1] Allen, P. M., Arnold, J. G., Auguste, L., White, J., and Dunbar, J.: Application of a simple headcut advance
495 model for gullies, *Hydrol. Earth Syst. Sci.*, 43, 202-217, <https://doi.org/10.1002/esp.4233>, 2018.
- 496 [2] Bierman, P. R. and Montgomery, D. R.: *Key Concepts in Geomorphology*, W. H. Freeman and Company
497 Publishers, ISBN 13:9781429238601, 2014.
- 498 [3] Dong, Y., Wu, Y., Yin, J., Wang, Y., and Gou, S.: Investigation of Soil Shear-Strength Parameters and Prediction
499 of the Collapse of Gully Walls in the Black Soil Region of Northeastern China, *Phys. Geogr.*, 32, 161-178,
500 <https://doi.org/10.2747/0272-3646.32.2.161>, 2011.
- 501 [4] Dong, Y., Wu, Y., Qin, W., Guo, Q., Yin, Z., and Duan, X.: The gully erosion rates in the black soil region of
502 northeastern China: Induced by different processes and indicated by different indexes, *Catena*, 182,
503 <https://doi.org/10.1016/j.catena.2019.104146>, 2019.
- 504 [5] Evans, D.: *Geomorphology: Critical Concepts in Geography - Volume IV, Glacial Geomorphology*, Routledge.,
505 ISBN 9780415641708, 2004.
- 506 [6] Fan, H., Hou, Y., Xu, X., Mi, C., and Shi, H.: Composite Factors during Snowmelt Erosion of Farmland in
507 Black Soil Region of Northeast China: Temperature, Snowmelt Runoff, Thaw Depths and Contour Ridge
508 Culture, *Water*, 15, <https://doi.org/10.3390/w15162918>, 2023.
- 509 [7] Farkas, C., Randriamampianina, R., and Majercak, J.: Modelling impacts of different climate change scenarios
510 on soil water regime of a Mollisol, *Cereal Res. Commun.*, 33, 185-188,
511 <https://doi.org/10.1556/crc.33.2005.1.45>, 2005.
- 512 [8] Gómez-Gutiérrez, A., Schnabel, S., De Sanjosé, J. J., and Contador, F. L.: Exploring the relationships between
513 gully erosion and hydrology in rangelands of SW Spain, *Z. Geomorphol.*, 56, 27-44,
514 <https://doi.org/10.1127/0372-8854/2012/s-00071>, 2012.
- 515 [9] Guan, Y., Yang, S., Zhao, C., Lou, H., Chen, K., Zhang, C., and Wu, B.: Monitoring long-term gully erosion
516 and topographic thresholds in the marginal zone of the Chinese Loess Plateau, *Soil Tillage Res.*, 205,
517 <https://doi.org/10.1016/j.still.2020.104800>, 2021.
- 518 [10] Guo, W., Xu, X., Wang, W., Zhu, T., and Liu, Y.: Experimental study of shallow mass movements on gully
519 slopes and associated sediment under rainfall on the Chinese loess plateau, *Geomorphology*, 350,
520 <https://doi.org/10.1016/j.geomorph.2019.106919>, 2020.
- 521 [11] Guo, W., Luo, L., Wang, W., Liu, Z., Chen, Z., Kang, H., and Yang, B.: Sensitivity of rainstorm-triggered
522 shallow mass movements on gully slopes to topographical factors on the Chinese Loess Plateau,
523 *Geomorphology*, 337, 69-78, <https://doi.org/10.1016/j.geomorph.2019.04.006>, 2019.
- 524 [12] Harmon, R. S. and Doe, W. W.: *Landscape erosion and evolution modeling*, Springer Science + Business Media,
525 New York., ISBN 978-1-4613-5139-9, 2001.
- 526 [13] Hayas, A., Peña, A., and Vanwallegem, T.: Predicting gully width and widening rates from upstream
527 contribution area and rainfall: A case study in SW Spain, *Geomorphology*, 341, 130-139,
528 <https://doi.org/10.1016/j.geomorph.2019.05.017>, 2019.
- 529 [14] Jiao, J., Qin, W., Li, K., Xu, H., Yin, Z., and Hou, S.: Critical thresholds for stage division of water erosion
530 process in different ridge systems in mollisol region of Northeast China, *J Mt. Sci.*, 20, 1540-1560,
531 <https://doi.org/10.1007/s11629-022-7476-5>, 2023.
- 532 [15] Kirkby, M. J. and Bracken, L. J.: Gully processes and gully dynamics, *Earth Surf. Process. Landf.*, 34, 1841-
533 1851, <https://doi.org/10.1002/esp.1866>, 2009.
- 534 [16] Li, H., Cruse, R. M., Liu, X., and Zhang, X.: Effects of Topography and Land Use Change on Gully
535 Development in Typical Mollisol Region of Northeast China, *Chin. Geogr. Sci.*, 26, 779-788,
536 <https://doi.org/10.1007/s11769-016-0837-7>, 2016.



- 537 [17] Li, H., Shen, H., Wang, Y., Wang, Y., and Gao, Q.: Effects of Ridge Tillage and Straw Returning on Runoff and
538 Soil Loss under Simulated Rainfall in the Mollisol Region of Northeast China, *Sustainability*, 13,
539 <https://doi.org/10.3390/su131910614>, 2021.
- 540 [18] Li, Z., Zhang, Y., Zhu, Q., He, Y., and Yao, W.: Assessment of bank gully development and vegetation coverage
541 on the Chinese Loess Plateau, *Geomorphology*, 228, 462-469, <https://doi.org/10.1016/j.geomorph.2014.10.005>,
542 2015.
- 543 [19] Li, Z., Zhang, Y., Zhu, Q., Yang, S., Li, H., and Ma, H.: A gully erosion assessment model for the Chinese Loess
544 Plateau based on changes in gully length and area, *Catena*, 148, 195-203,
545 <https://doi.org/10.1016/j.catena.2016.04.018>, 2017.
- 546 [20] Liu, X., Guo, M., Zhang, X., Zhang, S., Zhou, P., Chen, Z., Qi, J., and Shen, Q.: Morphological characteristics
547 and volume estimation model of permanent gullies and topographic threshold of gullying in the rolling hilly
548 Mollisols region of northeast China, *Catena*, 231, <https://doi.org/10.1016/j.catena.2023.107323>, 2023.
- 549 [21] Lu, N. and Godt, J. W.: *Hillslope Hydrology and Stability*, Cambridge University Press, Cambridge,
550 <https://doi.org/DOI:10.1017/CBO9781139108164>, 2013.
- 551 [22] Luffman, I. E., Nandi, A., and Spiegel, T.: Gully morphology, hillslope erosion, and precipitation characteristics
552 in the Appalachian Valley and Ridge province, southeastern USA, *Catena*, 133, 221-232,
553 <https://doi.org/10.1016/j.catena.2015.05.015>, 2015.
- 554 [23] Montgomery, D. R. and Dietrich, W. E.: Channel initiation and the problem of landscape scale, *Science*, 255,
555 826-830, <https://doi.org/10.1126/science.255.5046.826>, 1992.
- 556 [24] Mualem, Y.: Hysteretical models for prediction of the hydraulic conductivity of unsaturated porous media,
557 *Water Resour. Res.*, 12, 1248-1254, <https://doi.org/10.1029/WR012i006p01248>, 1976.
- 558 [25] Poesen, J., Vandaele, K., and van Wesemael, B.: Gully Erosion: Importance and Model Implications. In:
559 Boardman, J., Favis-Mortlock, D. (eds) *Modelling Soil Erosion by Water*. NATO ASI Series, vol 55. Springer,
560 Berlin, Heidelberg., https://doi.org/10.1007/978-3-642-58913-3_22, 1998.
- 561 [26] Poesen, J. W. A., Torri, D. B., and Vanwallegem, T.: Gully Erosion: Procedures to Adopt When Modelling Soil
562 Erosion in Landscapes Affected by Gullying, in: *Handbook of Erosion Modelling*, 360-386,
563 <https://doi.org/10.1002/9781444328455.ch19>, 2010.
- 564 [27] Rengers, F. K. and Tucker, G. E.: Analysis and modeling of gully headcut dynamics, North American high
565 plains, *J. Geophys. Res.-Earth Surf.*, 119, 983-1003, <https://doi.org/10.1002/2013jf002962>, 2014.
- 566 [28] Sidle, R. C., Gomi, T., Usuga, J. C. L., and Jarihani, B.: Hydrogeomorphic processes and scaling issues in the
567 continuum from soil pedons to catchments, *Earth Sci. Rev.*, 175, 75-96,
568 <https://doi.org/10.1016/j.earscirev.2017.10.010>, 2017.
- 569 [29] Stein, O. R. and Latray, D. A.: Experiments and modeling of head cut migration in stratified soils, *Water Resour.*
570 *Res.*, 38, 1284, <https://doi.org/10.1029/2001WR001166>, 2002.
- 571 [30] Svoray, T., Michailov, E., Cohen, A., Rokach, L., and Sturm, A.: Predicting gully initiation: comparing data
572 mining techniques, analytical hierarchy processes and the topographic threshold, *Earth Surf. Process. Landf.*,
573 37, 607-619, <https://doi.org/10.1002/esp.2273>, 2012.
- 574 [31] Tang, J., Xie, Y., Wu, Y., and Liu, G.: Influence of precipitation change and topography characteristics on the
575 development of farmland gully in the black soil region of northeast China, *Catena*, 224,
576 <https://doi.org/10.1016/j.catena.2023.106999>, 2023.
- 577 [32] Tang, J., Xie, Y., Liu, C., Dong, H., and Liu, G.: Effects of rainfall characteristics and contour tillage on
578 ephemeral gully development in a field in Northeastern China, *Soil Tillage Res.*, 218,
579 <https://doi.org/10.1016/j.still.2021.105312>, 2022.
- 580 [33] Tebebu, T. Y., Abiy, A. Z., Zegeye, A. D., Dahlke, H. E., Easton, Z. M., Tilahun, S. A., Collick, A. S., Kidnau,



- 581 S., Moges, S., Dadgari, F., and Steenhuis, T. S.: Surface and subsurface flow effect on permanent gully
582 formation and upland erosion near Lake Tana in the northern highlands of Ethiopia, *Hydrol. Earth Syst. Sci.*,
583 14, 2207-2217, <https://doi.org/10.5194/hess-14-2207-2010>, 2010.
- 584 [34] Thomas, J. T., Iverson, N. R., and Burkart, M. R.: Rank-collapse processes in a valley-bottom gully, western
585 Iowa, *Earth Surf. Process. Landf.*, 34, 109-122, <https://doi.org/10.1002/esp.1699>, 2009.
- 586 [35] Torri, D. and Poesen, J.: A review of topographic threshold conditions for gully head development in different
587 environments, *Earth Sci. Rev.*, 130, 73-85, <https://doi.org/10.1016/j.earscirev.2013.12.006>, 2014.
- 588 [36] van Beek, R., Cammeraat, E., Andreu, V., Mickovski, S. B., and Dorren, L.: Hillslope Processes: Mass Wasting,
589 Slope Stability and Erosion, in: *Slope Stability and Erosion Control: Ecotechnological Solutions*, edited by:
590 Norris, J. E., Stokes, A., Mickovski, S. B., Cammeraat, E., van Beek, R., Nicoll, B. C., and Achim, A., Springer
591 Netherlands, Dordrecht, 17-64, https://doi.org/10.1007/978-1-4020-6676-4_3, 2008.
- 592 [37] van Genuchten, M. T.: A Closed-form Equation for Predicting the Hydraulic Conductivity of Unsaturated Soils,
593 *Soil Sci. Soc. Am. J.*, 44, 892-898, <https://doi.org/10.2136/sssaj1980.03615995004400050002x>, 1980.
- 594 [38] Vanmaercke, M., Poesen, J., Van Mele, B., Demuzere, M., Bruynseels, A., Golosov, V., Bezerra, J. F. R.,
595 Bolysov, S., Dvinskikh, A., Frankl, A., Fuseina, Y., Guerra, A. J. T., Haregeweyn, N., Ionita, I., Imwangana, F.
596 M., Moeyersons, J., Moshe, I., Samani, A. N., Niacsu, L., Nyssen, J., Otsuki, Y., Radoane, M., Rysin, I., Ryzhov,
597 Y. V., and Yermolaev, O.: How fast do gully headcuts retreat?, *Earth Sci. Rev.*, 154, 336-355,
598 <https://doi.org/10.1016/j.earscirev.2016.01.009>, 2016.
- 599 [39] Wang, J., Zhang, Y., Deng, J., Yu, S., and Zhao, Y.: Long-Term Gully Erosion and Its Response to Human
600 Intervention in the Tableland Region of the Chinese Loess Plateau, *Remote Sens.*, 13,
601 <https://doi.org/10.3390/rs13245053>, 2021a.
- 602 [40] Wang, L., Zheng, F., Liu, G., Zhang, X., Wilson, G. V., Shi, H., and Liu, X.: Seasonal changes of soil erosion
603 and its spatial distribution on a long gentle hillslope in the Chinese Mollisol region, *Int. Soil Water Conserv.*
604 *Res.*, 9, 394-404, <https://doi.org/10.1016/j.iswcr.2021.02.001>, 2021b.
- 605 [41] Wang, Z., Liu, B., Wang, X., Gao, X., and Liu, G.: Erosion effect on the productivity of black soil in Northeast
606 China, *Sci. China Ser. D-Earth Sci.*, 52, 1005-1021, <https://doi.org/10.1007/s11430-009-0093-0>, 2009.
- 607 [42] Wayllace, A. and Lu, N.: A Transient Water Release and Imbibitions Method for Rapidly Measuring Wetting
608 and Drying Soil Water Retention and Hydraulic Conductivity Functions, *Geotech. Test. J.*, 35, 103-117,
609 <https://doi.org/10.1520/GTJ103596>, 2012.
- 610 [43] Wen, Y., Kasielke, T., Li, H., Zepp, H., and Zhang, B.: A case-study on history and rates of gully erosion in
611 Northeast China, *Land Degrad. Dev.*, 32, 4254-4266, <https://doi.org/10.1002/ldr.4031>, 2021.
- 612 [44] Wen, Y., Liu, B., Jiang, H., Li, T., Zhang, B., and Wu, W.: Initial soil moisture prewinter affects the freeze-thaw
613 profile dynamics of a Mollisol in Northeast China, *Catena*, 234, <https://doi.org/10.1016/j.catena.2023.107648>,
614 2024.
- 615 [45] Xu, X., Zheng, F., Wilson, G. V., and Wu, M.: Upslope inflow, hillslope gradient and rainfall intensity impacts
616 on ephemeral gully erosion, *Land Degrad. Dev.*, 28, 2623-2635, <https://doi.org/10.1002/ldr.2825>, 2017.
- 617 [46] Xu, X., Zheng, F., Wilson, G. V., He, C., Lu, J., and Bian, F.: Comparison of runoff and soil loss in different
618 tillage systems in the Mollisol region of Northeast China, *Soil Tillage Res.*, 177, 1-11,
619 <https://doi.org/10.1016/j.still.2017.10.005>, 2018.
- 620 [47] Xu, X., Ma, Y., Yang, W., Zhang, H., Tarolli, P., Jiang, Y., and Yan, Q.: Qualifying mass failures on loess gully
621 sidewalls using laboratory experimentation, *Catena*, 187, <https://doi.org/10.1016/j.catena.2019.104252>, 2020.
- 622 [48] Yang, J., Zhang, S., Chang, L., Li, F., Li, T. Q., and Gao, Y.: Gully erosion regionalization of black soil area in
623 northeastern China, *Chin. Geogr. Sci.*, 27, 78-87, <https://doi.org/10.1007/s11769-017-0848-z>, 2017.
- 624 [49] Zare, M., Soufi, M., Nejabat, M., and Pourghasemi, H. R.: The topographic threshold of gully erosion and



- 625 contributing factors, *Nat. Hazard*, 112, 2013-2035, <https://doi.org/10.1007/s11069-022-05254-6>, 2022.
- 626 [50] Zhang, S., Jiang, L., Liu, X., Zhang, X., Fu, S., and Dai, L.: Soil nutrient variance by slope position in a Mollisol
627 farmland area of Northeast China, *Chin. Geogr. Sci.*, 26, 508-517, <https://doi.org/10.1007/s11769-015-0737-2>,
628 2016.
- 629 [51] Zhang, S., Wang, X., Xiao, Z., Qu, F., Wang, X., Li, Y., Aurangzeib, M., Zhang, X., and Liu, X.: Quantitative
630 studies of gully slope erosion and soil physiochemical properties during freeze-thaw cycling in a Mollisol region,
631 *Sci. Total Environ.*, 707, <https://doi.org/10.1016/j.scitotenv.2019.136191>, 2020.
- 632 [52] Zhang, S., Han, X., Cruse, R., Zhang, X., Hu, W., Yan, Y., and Guo, M.: Morphological characteristics and
633 influencing factors of permanent gully and its contribution to regional soil loss based on a field investigation of
634 393 km² in Mollisols region of northeast China, *Catena*, 217, <https://doi.org/10.1016/j.catena.2022.106467>,
635 2022.
- 636 [53] Zhou, P., Guo, M., Zhang, X., Zhang, S., Qi, J., Chen, Z., Wang, L., and Xu, J.: Quantifying the effect of freeze-
637 thaw on the soil erodibility of gully heads of typical gullies in the Mollisols region of Northeast China, *Catena*,
638 228, <https://doi.org/10.1016/j.catena.2023.107180>, 2023.